120 GBd 2.8 $V_{pp,diff}$ Low-Power Differential Driver for InP Mach–Zehnder Modulator Using 55-nm SiGe HBTs

Jung Han Choi, *Member, IEEE*, and Nisarg Nijanandi

***Abstract*— We present a 120 GBd 2.8 $V_{pp,diff}$ driver for InP Mach–Zehnder modulator (MZM) using 55-nm SiGe heterojunction bipolar transistor (HBTs). The output impedance of the driver has a differential 2 × 25 Ω, matched to the optical modulator. The measured 3-dB bandwidth exceeds 67 GHz, and the output $P_{1\,dB}$ is about 16.7 dBm at 1 GHz. The variable gain using the Gilbert-cell is implemented, and a 2.1 dB gain variation is measured. The total harmonic distortion (THD) is 2.5% at 1 GHz. The power consumption is 960 mW. The eye openings up to 120 GBd are characterized by exploiting the impedance conversion integrated circuit (IC), which is de-embedded afterward. The post-processing of the de-embedding results in the rail-to-rail voltage output of 2.8 $V_{pp,diff}$.**

***Index Terms*— 120 GBd, baud rate, de-embedding, heterojunction bipolar transistor (HBT), impedance conversion, Mach–Zehnder, SiGe.**

I. Introduction

RECENT considerable efforts to increase the baud rate of the optical transmission system led to the development of high-speed electronics for the optical transmitter and receiver modules. With regard to the optical transmitter, the InP-based ultrahigh-speed modulator requires, in fact, very high-swing driving voltages, e.g., 3.0 $V_{pp,diff}$ for InP Mach–Zehnder modulator (MZM) with 2 × 25 Ω load conditions [1]. The driver for the InP MZM inevitably consumes high power due to the small impedance of the MZM. Thus, great attention have been made to reducing power consumption of the driver circuitry using the codesign technique [1]. In addition, to reduce RF losses in the module, lots of discussions are underway in the Optical Internet Working Forum (OIF) for 128 GBd [2].

The next generation of the optical transceiver will support more than 100 GBd. To achieve such a high baud rate, different materials for the optical modulator such as InP MZM, plasmonic organic hybrid MZM, silicon photonics MZM, and $LibNO_3$ modulators [3], have been demonstrated and are still research themes. Drivers for each modulator have been investigated using either InP- or SiGe-based heterojunction bipolar transistor (HBTs). Depending on the operation principle of each modulator, the different driver configuration has been considered. In the case of the InP MZM, since the characteristic impedance is differential 2 × 25 Ω [1], the driving voltage requires higher current than the conventional 2 × 50 Ω, thus the output stage of the driver shall tolerate high current, maintaining high RF performance.

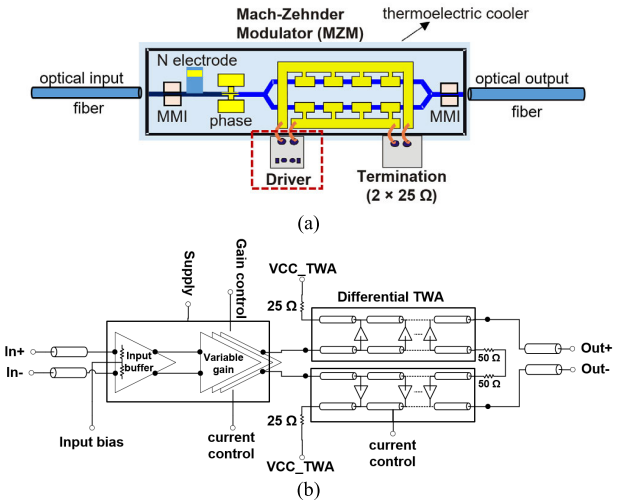

Fig. 1. (a) Block diagram of an optical transmitter. (b) Driver architecture for InP MZM [4].

In this letter, we report on the low-power 120 GBd 2.8 $V_{pp,diff}$ driver for InP MZM using 50-nm SiGe HBT technology. The integrated circuit (IC) is composed of an input buffer, a variable-gain amplifier, and a post-amplifier using the traveling-wave configuration. The output impedance is designed to have 2 × 25 Ω in order to match the impedance of the InP MZM. Time-domain measurement technique including the impedance conversion IC is discussed in detail.

II. Driver Architecture

A. Driver Architecture

Fig. 1(a) displays the block diagram of the optical transmitter module based on the InP-based MZM. It is composed of the MZM, a thermoelectric cooler (TEC), a driver, and the termination chip. The power consumption of the driver can lead to thermal coupling to the MZM. Therefore, when the power is high enough to cause the thermal problem, the driver shall be mounted onto the TEC. In turn, it will increase the power of the active TEC. Fig. 1(b) illustrates the driver architecture. The input buffer for the input matching is located in front of the variable gain amplifier (VGA). The output signals from the VGA will feed through to the traveling-wave amplifier (TWA) and encounter 2 × 50 Ω input termination at the input end of the TWA. The outputs of the TWA are

Manuscript received 23 February 2023; revised 6 April 2023; accepted 10 April 2023. *(Corresponding author: Jung Han Choi.)*

The authors are with the Fraunhofer Heinrich-Hertz Institute, 10587 Berlin, Germany (e-mail: jung-han.choi@hhi.fraunhofer.de).

This article was presented at the IEEE MTT-S International Microwave Symposium (IMS 2023), San Diego, CA, USA, June 11–16, 2023.

Color versions of one or more figures in this letter are available at https://doi.org/10.1109/LMWT.2023.3271850.

Digital Object Identifier 10.1109/LMWT.2023.3271850

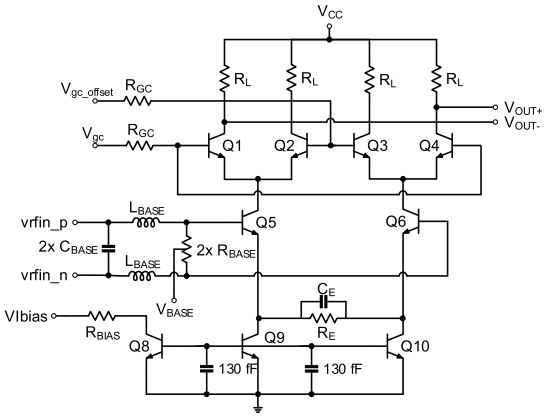

Fig. 2. Schematic of the Gilbert-cell-based VGA.

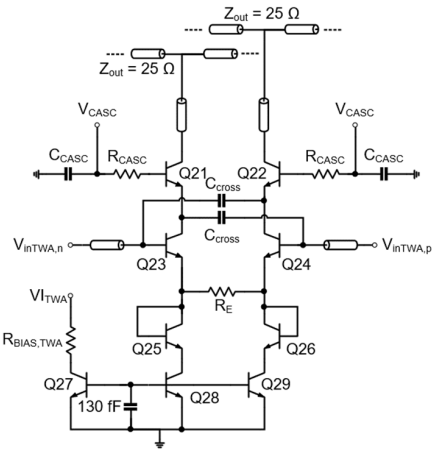

Fig. 3. Circuit schematic of TWA cell.

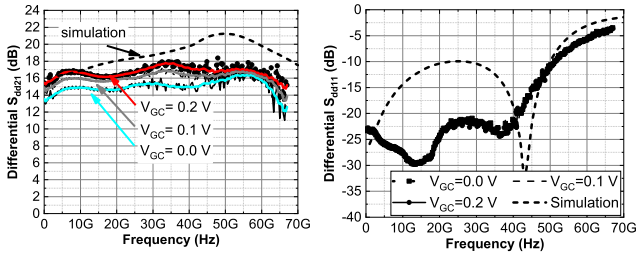

(a) (b)

Fig. 4. Differential large-signal S-parameter results. (a) S_{dd21}. (b) S_{dd11}.

terminated with 2 × 25 Ω in order to match the characteristic impedance of the MZM. Using the electro-optical codesign technique, the differential impedance of the MZM has been determined [1] to minimize the power consumption of the overall optical transmitter.

III. Circuit Implementations

A. Variable Gain Amplifier

The driver is fabricated using the 50-nm SiGe HBT technology, which has f_T and f_{MAX} of 320 and 370 GHz, respectively. The transistors used in the driver have breakdown voltages of 1.5 V for BV_{CEO} and 5.2 for BV_{CBO}, respectively. The VGA is composed of the Gilbert-cell, as shown in Fig. 2. According to [5], the voltage gain in the Gilbert-cell can be expressed as follows:

$$A_V = \frac{V_{\text{out}}}{V_{\text{in}}} = \frac{R_L}{Z_E}\tanh\left(\frac{V_{\text{GC}}}{2V_T}\right)$$

where V_{in} = vrfin_p-vrfin_n, $Z_E = R_E//C_E$, $V_{\text{GC}} = V_{\text{gc}}-V_{\text{gc\_offset}}$, and $V_T = kT/q = 25.8$ mV. According to the simulation results, the gain variation is about 3 dB when V_{GC} ranges from −0.25 to 0 V. The input matching is made of the resistance, inductance, and capacitance, as shown in Fig. 2. The parasitic components of resistance (R_{BASE}) at the base of $Q5$ and $Q6$ hinder broadband matching characteristics. Therefore, series L (L_{BASE}) and shunt C (C_{BASE}) are additionally added to the input ports. The S_{dd11} simulation result shows <−10 dB up to 45 GHz. The emitter degenerate resistance (R_E) and capacitance (C_E) have been exploited to increase the bandwidth of the VGA.

1) Traveling-Wave Amplifier

Fig. 3 shows the single amplifier cell of the TWA. To support high output voltage and increase the output impedance of the amplifier cell seen in the collector of $Q21$ and $Q22$, the cascode configuration has been chosen. The target specification is to deliver an output swing of >2.5 $V_{\text{pp,diff}}$ when the load is 2 × 25 Ω. The input transmission line is a coupled differential line, which has 2 × 50 Ω termination resistances at the end of the line. The width and the gap of the line are 14.3 and 5.5 μm, respectively. The cross-coupling capacitor (C_{cross}) has been optimized to enhance the bandwidth of the circuit. The cascode resistance (R_{CASC}) and capacitance (C_{CASC}) are determined to ensure that the driver stability factor is larger than 1 up to 100 GHz. The output transmission line shall have a 25 Ω characteristic impedance. The width of the line is 10 μm. Special care has been paid to the 25 Ω output termination resistance layout since each should flow about 40 mA in dc. The necessary wider metal and resistance width in turn lead to increased parasitics, deteriorating the frequency response in high frequency. After several optimizations, the resistance layout and the transmission line dimension are determined.

IV. Measurements

A. Differential Large-Signal S-Parameters

After performing the power calibration (from −10 to 0 dBm) and the on-wafer calibration using the short-open-load-thru (SOLT) technique, the differential *large-signal* S-parameters have been measured using the network analyzer (Rohde&Schwarz ZVA 65). The results for true-differential S-parameters are presented in Fig. 4. Since the output impedance of the driver is 2 × 25 Ω, the network analyzer is configured at the output differential port to have differential and common-mode impedances of 50 and 12.5 Ω, respectively. Using different V_{GC} voltages, the S_{dd21} and S_{dd11} are measured when the differential input power is −5 dBm. The 3-dB bandwidths are larger than 67 GHz, regardless of V_{GC}. And, the differential input reflections [Fig. 4(b)] show no influence by the V_{GC} variations. S_{dd11} shows −10 dB up to 50 GHz.

B. Nonlinearity Measurements

Nonlinearity characteristics are measured using the output $P_{1\,\text{dB}}$ compression and total-harmonic distortion (THD). The output $P_{1\,\text{dB}}$ results are displayed in Fig. 5(a) and (b). All measurements are carried out at 45 °C. The output $P_{1\,\text{dB}}$ at $V_{\text{GC}} = 0.2$ V is 16.7 dBm at 1 GHz for the load impedance of $Z_L = 2 \times 25$ Ω. Further measurements up to 30 GHz show relative constant results of 17 ± 1 dBm [see Fig. 5(b)]. The THD measurements are also done under 45 °C since the optical transmitter module is assumed to operate at such environment in the system rack. Using the spectrum analyzer (HP 8565E), the power of each spectral component up to the

TABLE I
PERFORMANCE COMPARISON WITH STATE-OF-THE-ART OPTICAL MODULATOR DRIVER

Ref.	Bandwidth (GHz)	Data rate (GBd)	Technology	Output (V_{pp})	Load impedance	Output (differential)	Driver type	Optical component (load)	Power (W)
[6]	-	140	SiGe HBT 150nm	2	capacitive load	diff.	Multiplexer	Plasmonic organic hybrid MZM	7.15
[7]		222	InP DHBT	0.24/0.73	capacitive load	diff.	2:1 multiplexing selector	Plasmonic organic hybrid MZM	0.5 / 0.8
[8]		100	SiGe HBT 180 nm	-	-	-	-	InP MZM	-
[9][10]	> 67	128 (176)	InP DHBT	1.5	**2x 25 Ohm**	diff.	lumped + distributed	InP MZM	0.84
[11]	> 70	56	SiGe HBT 55nm	4.8	2x 50 Ohm	diff.	distributed	-	1.1
[12]	90	120	SiGe HBT 130 nm	4	2x 50 Ohm	diff.	distributed	-	0.55
[13]	57.5	56	SiGe HBT 55nm	3.8	2x 50 Ohm	diff.	lumped	Silicon Photonic MZM	0.82
This work	**> 67**	**120**	**SiGe HBT 55nm**	**2.8**	**2x 25 Ohm**	**diff.**	**lumped + distributed**	**InP MZM**	**0.96**

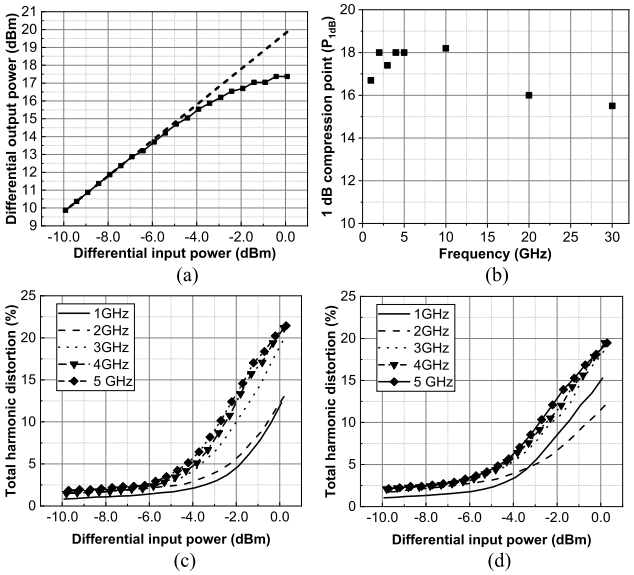

Fig. 5. (a) Output $P_{1\,dB}$ results at 1 GHz ($Z_L = 2 \times 25\ \Omega$) under 45 °C. (b) Measured output $P_{1\,dB}$ at various frequencies. (c) and (d) Measured THD for $V_{GC} = 0.1$ V and $V_{GC} = 0.2$ V, respectively, under 45 °C.

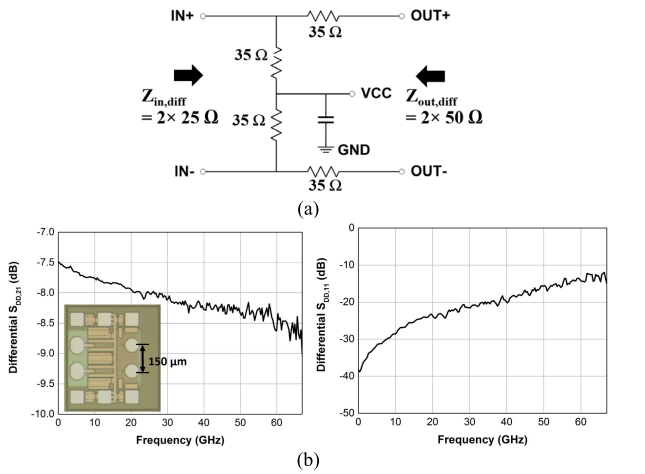

Fig. 6. (a) Schematic of impedance conversion IC. (b) Measured differential S_{dd21} and S_{dd11} results and its photograph.

fifth harmonics is measured for a 50-Ω load and recalculated for a 25-Ω load. For the two bias conditions, the results are measured and presented in Fig. 5(c) and (d), respectively. At 1 GHz, the THD remains below 2.5% when the differential input power is −5 dBm. This power level is equivalent to the *large-signal* S-parameter measurement condition. Up to 5 GHz, the measured THD remains lower than 5%.

C. Time-Domain Measurements

Since the output impedance of the driver is 2 × 25 Ω, the transient outputs are hard to be measured precisely due to the impedance mismatch with the 50-Ω instrument. Therefore, the impedance-conversion IC (ICIC) has been developed to convert from 2 × 25 Ω to 2 × 50 Ω. It is composed of resistors, as shown in Fig. 6(a). S_{dd21} and S_{dd11} results are provided in Fig. 6(b). The 3-dB frequency is larger than 67 GHz and S_{dd11} remains below −15 dB up to 55 GHz. The driver and the ICIC are connected using the Au wire bonds with a 24 μm diameter [Fig. 7(a)] and the length of 250 μm is measured. It is modeled with the π-equivalent circuit, composed of a series L and two shunt Cs. By comparing measured S-parameters with the modeling result, the L is estimated at about 240 pH and the C is about 0–20 fF. The measured S_{dd21} after wire-bonding with ICIC is −7.5 dB lower than that of the driver, since the ICIC has −7.5 dB inherent loss. The 3- and 6-dB frequencies are characterized to be 34 and 50 GHz, respectively.

Fig. 7(b) shows the measurement setup for the transient output measurements for the module. The high-speed digital signals are generated using the 2:1 multiplexer (SHF C603A), combined with the bit pattern generator (BPG, SHF 12105A). The RF probes (Formfactor, infinity-probe) have 1.85 mm (V-type), namely speaking, valid up to 67 GHz. All RF components at the output are independently measured in frequency domain in order to perform de-embedding. The reference plane for the de-embedding is up to the ICIC. It means that the de-embedded output signals will include the effect of 240 pH wire bonding. The RF probes, cables, and the ICIC are de-embedded in the time domain to reconstruct the output signal from the driver. The rail-to-rail differential output is measured to be 2.8 $V_{pp,diff}$ up to 120 GBd as shown in Fig. 8 when the load is 2 × 25 Ω. It shall be noted that the eye openings can be improved after excluding the wire-bonding parasitics. The state-of-the-art is summarized in Table I.

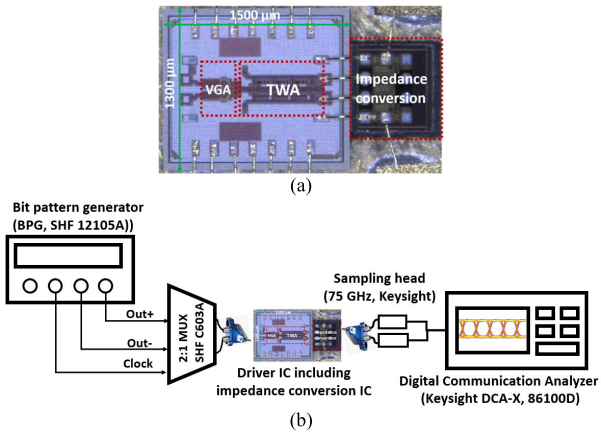

Fig. 7. (a) Photograph of module for time-domain measurement. (b) Measurement setup for time-domain measurement.

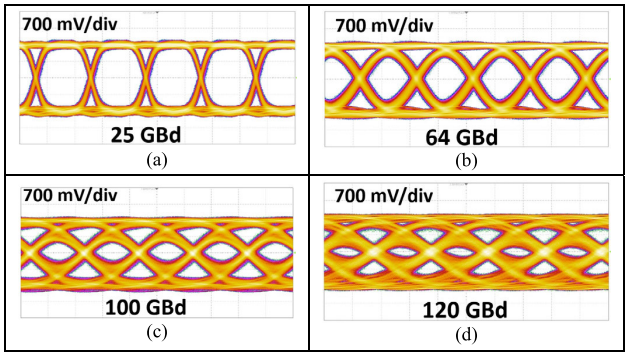

Fig. 8. Measurement results of eye openings at various baud rates. (a) 25 GBd, (b) 64 GBd, (c) 100 GBd, and (d) 120 GBd.

V. Conclusion

We have successfully demonstrated 120 GBd 2.8 $V_{\mathrm{pp,diff}}$ driver for InP MZM using 50-nm SiGe HBT. The driver showed more than 67-GHz bandwidth, a maximum differential gain of 16.5 dB, a gain variation of 2 dB, a THD of 2.5% at 1 GHz, and the power consumption of 960 mW.

References

[1] J. H. Choi, "Ultra-low power SiGe driver-IC for high-speed InP Mach–Zehnder modulator," in *High-Speed and Lower Power Technologies: Electronics and Photonics* (Devices, Circuits, and Systems), J. H. Choi, and K. Iniewski, Eds. London, U.K.: CRC Press, 2020, ch. 8, pp. 187–210.

[2] *High Bandwidth Coherent Driver Modulator (HB-CDM) 2.0*. Accessed: May 3, 2023. [Online]. Available: https://www.oiforum.com/technical-work/hot-topics/high-bandwidth-coherent-driver-modulator-hb-cdm-2-0/

[3] B. J. Khurgin, "Comparison of charge and field driven optical modulators," *Proc. SPIE*, vol. PC12195, Oct. 2022, Art. no. PC121951G.

[4] H. Wakita, M. Nagatani, K. Kurishima, M. Ida, and H. Nosaka, "An over-67-GHz-bandwidth 2 V_{pp} linear differential amplifier with gain control in 0.25-μm InP DHBT technology," in *IEEE MTT-S Int. Microw. Symp. Dig.*, May 2016, pp. 1–3.

[5] A. B. Grebene, *Bipolar and MOS Analog Integrated Circuit Design*. Hoboken, NJ, USA: Wiley, 2003, ch. 8.

[6] C. Uhl, H. Hettrich, and M. Moller, "Design considerations for a 100 Gbit/s SiGe-BiCMOS power multiplexer with 2 V_{pp} differential voltage swing," *IEEE J. Solid-State Circuits*, vol. 53, no. 9, pp. 2479–2487, Sep. 2018.

[7] W. Heni et al., "Ultra-high-speed 2:1 digital selector and plasmonic modulator IM/DD transmitter operating at 222 GBaud for intra-datacenter applications," *J. Lightw. Technol.*, vol. 38, no. 9, pp. 2734–2739, May 1, 2020.

[8] R. W. Going et al., "1.00 (0.88) Tb/s per wave capable coherent multi-channel transmitter (receiver) InP-based PICs with hybrid integrated SiGe electronics," *IEEE J. Quantum Electron.*, vol. 54, no. 4, pp. 1–10, Aug. 2018.

[9] Y. Ogiso et al., "80-GHz bandwidth and 1.5-V vπ InP-based IQ modulator," *J. Lightw. Technol.*, vol. 38, no. 2, pp. 249–255, Jan. 15, 2020.

[10] *NTT Achieves the World's Fastest Optical Transmission of over 2 Tbits/s Per Wavelength*. Accessed: May 3, 2023. [Online]. Available: https://group.ntt/en/newsrelease/2022/09/22/220922a.html

[11] R. J. A. Baker, J. Hoffman, P. Schvan, and S. P. Voinigescu, "SiGe BiCMOS linear modulator drivers with 4.8-Vpp differential output swing for 120-GBaud applications," in *Proc. IEEE Radio Freq. Integr. Circuits Symp. (RFIC)*, Jun. 2017, pp. 260–263.

[12] P. Rito, I. G. López, A. Awny, M. Ko, A. C. Ulusoy, and D. Kissinger, "A DC-90-GHz 4-Vpp modulator driver in a 0.13-μm SiGe:C BiCMOS process," *IEEE Trans. Microw. Theory Techn.*, vol. 65, no. 12, pp. 5192–5202, Dec. 2017.

[13] A. Zandieh, P. Schvan, and S. P. Voinigescu, "Linear large-swing push–pull SiGe BiCMOS drivers for silicon photonics modulators," *IEEE Trans. Microw. Theory Techn.*, vol. 65, no. 12, pp. 5355–5366, Dec. 2017.